Phase properties of the optical near field

R. Carminati*

Instituto de Ciencia de Materiales, Consejo Superior de Investigaciones Cientificas, Cantoblanco, 28049 Madrid, Spain

(Received 30 January 1997)

This paper presents a theoretical and numerical study of the phase properties of the optical near field. A model based on the first Rytov approximation for three-dimensional electromagnetic vector fields describes the relationship between the phase variations and both the topographic and optical properties of the scatterer. It is shown that strong polarization effects can lead to subwavelength phase variations around nanometric structures. The conclusions of the model are illustrated by exact numerical calculations. This study should find broad experimental applications in near-field optical interferometric phase measurements. [S1063-651X(97)51705-3]

PACS number(s): 45.25.Fx, 07.79.Fc, 61.16.Ch, 03.80.+r

Optical resolution beyond the Rayleigh (or diffraction) limit can be achieved by detecting the electromagnetic field at subwavelength distance from the object [1]. This has opened new perspectives for light microscopy with the development of scanning near-field optical microscopy (SNOM) [2]. In SNOM, a tip of subwavelength dimension (either illuminating or detecting) is placed at subwavelength distance from the object. The scattering process transfers part of the light energy from the near zone to the far zone. Recording the far-field energy versus the relative tip-sample position provides the image. The key point in this technique is the conversion of evanescent waves into propagating waves, which allows one to overcome the diffraction limit. In order to understand the properties of the optical near field, a lot of work has been concentrated on the description of the light intensity (often assumed to be the square modulus of the electric field) in close proximity of scatterers of arbitrary shape and composition [3]. Light confinement and polarization effects around nanometric structures have been described by different theoretical approaches [4–6] and observed with a photon scanning tunneling microscope [7].

Recently, interferometric measurements have provided a way to record the phase of the near field, in the microwave regime [8], and with visible light [9,10]. These new kinds of near-field optical measurements are promising, since a nanometric resolution was obtained with the set up of Ref. [9]. The first theoretical study of the phase properties in SNOM was presented in Ref. [11]. A scalar model showed that such a resolution was strongly dependent on the sample properties (refractive index and topography). Moreover, this model put forward that the phase of the scattered near field should closely follow the surface profile (in the case of a homogeneous sample). It was stated that phase measurements could represent a breakthrough in SNOM [11].

In this paper, we will study the near-field phase properties with a model based on the Rytov approximation for three-dimensional vector fields [12]. It will be shown that, under certain conditions that are strongly dependent on the polarization of the incident field, the phase of the scattered field closely follows an ''equivalent surface profile.'' This equivalent profile connects the topographic and dielectric properties of the scatterer. Subwavelength phase variations (''phase confinement'') and polarization effects will be demonstrated in order to put forward the power and the limitations of near-field phase imaging. The conclusions of our model will be illustrated by exact numerical calculations of the near field scattered by two-dimensional structures.

Let us consider a three-dimensional sample consisting of a flat interface separating a vacuum ($z>0$) from a homogeneous substrate of (frequency dependent) dielectric constant ϵ_s ($z<0$). An inhomogeneous object described by its topographic profile $z=S(x,y)$ and its (frequency-dependent) dielectric constant $\epsilon(x,y,z)$ is deposited on the interface. An example of such a sample is shown in Fig. 1. When this system is illuminated by an incident monochromatic field of wavelength λ, the total field for $z>S(x,y)$ obeys the Lippmann-Schwinger equation [13] (a temporal dependence $\exp(-i\omega t)$ is assumed for all fields):

$$\mathbf{E}(\mathbf{r})=\mathbf{E}^{(0)}(\mathbf{r})+k_0^2\int [\epsilon(\mathbf{r}')-1]\overleftrightarrow{\mathbf{G}}(\mathbf{r}_\parallel-\mathbf{r}'_\parallel,z,z')\mathbf{E}(\mathbf{r}')d^3\mathbf{r}'. \tag{1}$$

$\overleftrightarrow{\mathbf{G}}$ is the Green dyadic for the system with flat interface at $z=0$, $\mathbf{E}^{(0)}$ is the field that would exist in this system (i.e., without the object). The integral describes the scattered field

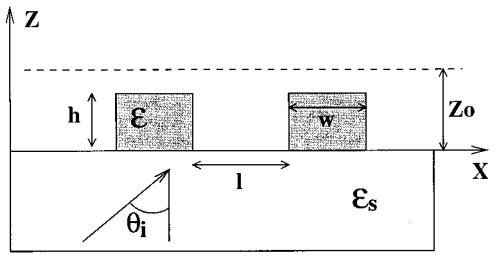

FIG. 1. Example of scattering system. The theoretical model applies to three-dimensional geometries. The system represented here is the one used in the two-dimensional numerical simulations, and is invariant in the y direction.

*Electronic address: rcarmina@icmm.csic.es

and is extended to the volume of the object. The notations $\mathbf{r}=(x,y,z)$, $\mathbf{r}_\parallel=(x,y)$, and $k_0=\omega/c=2\pi/\lambda$ are used.

When the object has a smooth profile [$h=\sup|S(x,y)|\ll\lambda$] and a low dielectric contrast $\Delta\epsilon=\epsilon(\mathbf{r})-1$ (this is expected to be the case with most of the sample studied in SNOM), the first Rytov approximation can be used to describe the scattered field [14]. We write the α component of the *total* field in the form

$$E_\alpha(\mathbf{r})=E_\alpha^{(0)}(\mathbf{r})\exp[\phi_\alpha(\mathbf{r})]\simeq E_\alpha^{(0)}(\mathbf{r})[1+\phi_\alpha^{(1)}(\mathbf{r})]. \quad (2)$$

Note that Eq. (2) implies that each component of the electric field is scattered independently. This means that no energy is transferred from one component to another during the scattering process. This hypothesis is consistent with the weak scattering assumption, and will be confirmed below by the numerical simulations. Equations (1) and (2) lead to (in the first Rytov approximation) [14]:

$$\phi_\alpha^{(1)}(\mathbf{r})=\frac{k_0^2}{E_\alpha^{(0)}(\mathbf{r})}\int[\epsilon(\mathbf{r}')-1]G_{\alpha\alpha}(\mathbf{r}_\parallel-\mathbf{r}'_\parallel,z,z')\times E_\alpha^{(0)}(\mathbf{r}')d^3\mathbf{r}'. \quad (3)$$

The integral in Eq. (3) corresponds to the first Born approximation for the α component in Eq. (1). To proceed further, we expand this integral to first order in h/λ. This leads to (see Ref. [15] for more details):

$$\phi_\alpha^{(1)}(\mathbf{r})=\frac{k_0^2}{E_\alpha^{(0)}(\mathbf{r})}(\epsilon_s-1)\int G_{\alpha\alpha}(\mathbf{r}_\parallel-\mathbf{r}'_\parallel,z,0)\times E_\alpha^{(0)}(\mathbf{r}'_\parallel,0)S_{eq}(\mathbf{r}'_\parallel)d^2\mathbf{r}'_\parallel, \quad (4)$$

where the integral is now a surface integral extended to the entire x-y plane. S_{eq} is an equivalent surface profile connecting the dielectric constant variation and the topography of the object [15]:

$$S_{eq}(\mathbf{r}_\parallel)=(\epsilon_s-1)^{-1}\int_0^{S(\mathbf{r}_\parallel)}[\epsilon(\mathbf{r}_\parallel,z)-1]dz. \quad (5)$$

In the case of a homogeneous sample ($\epsilon=\epsilon_s$), S_{eq} reduces to the true topographic profile.

Equation (4) is our starting point for a discussion of the phase properties in the near field. Im($\phi_\alpha^{(1)}$) (Im denoting the imaginary part) is the phase difference between the α component of the *total* field and the α component of the illuminating field $\mathbf{E}^{(0)}$. Equation (4) describes how this phase difference is connected to the properties of the object (the latter being described by S_{eq}). The resemblance (or lack of it) between Im($\phi_\alpha^{(1)}$) and S_{eq} strongly depends on the illuminating field and the direction of the α component of the field with respect to the (eventual) privileged directions of the equivalent surface profile. This leads to *phase* polarization and confinement effects, as those observed in the intensity (i.e., $|\mathbf{E}|^2$) [4–7]. Let us consider the simple case in which the illuminating field is a transmitted plane wave at normal incidence, $\mathbf{E}^{(0)}(\mathbf{r})=\mathbf{E}_0\exp(ik_0z)$. Equation (4) becomes

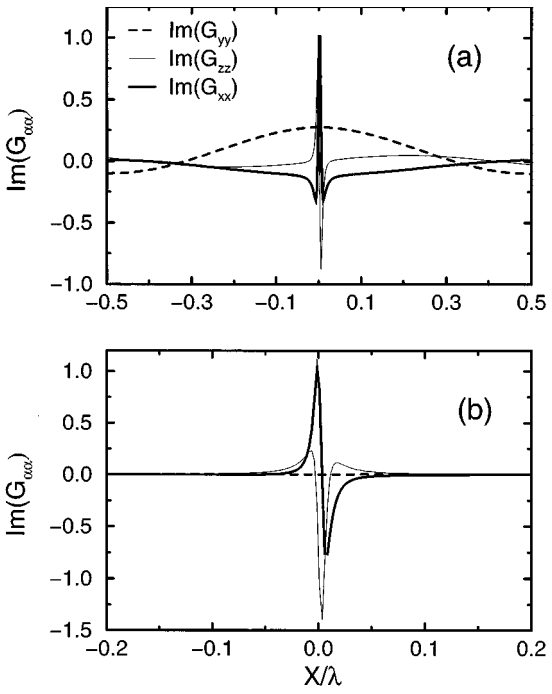

FIG. 2. Imaginary part of the components of the Green dyadic versus x. $y=0$ and $z_0=6$ nm. (a) $\theta_i=0°$. (b) $\theta_i=50°$ (total internal reflection).

$$\phi_\alpha^{(1)}(\mathbf{r}_\parallel,z_0)=\frac{k_0^2}{\exp(ik_0z_0)}(\epsilon_s-1)\times\int G_{\alpha\alpha}(\mathbf{r}_\parallel-\mathbf{r}'_\parallel,z_0,0)S_{eq}(\mathbf{r}'_\parallel)d^2\mathbf{r}'_\parallel, \quad (6)$$

where we have assumed that the phase was measured in a plane $z=z_0$. The relationship between the phase difference Im($\phi_\alpha^{(1)}$) and the object properties S_{eq} is governed by the imaginary part of the components $G_{\alpha\alpha}$ of the Green dyadic. They are plotted in Fig. 2, versus x, for $y=0$ and $z_0=6$ nm. According to Eq. (6), the convolution of Im($G_{\alpha\alpha}$) by the equivalent surface profile S_{eq} gives the phase variation. At normal incidence [Fig. 2(a)], Im(G_{xx}) is sharply peaked around $x=0$ (and symmetric), so that the phase Im($\phi_x^{(1)}$) will closely follow the equivalent surface profile. Subwavelength phase variations (''phase confinement'') will be observed around the inhomogeneities of the object. On the contrary, Im(G_{yy}) has a width of about one wavelength, eliminating the possibility of subwavelength resolution with phase imaging. The case of G_{zz} is not worth being discussed because at normal incidence, the z component of the scattered field is so weak that a measurement of $\phi_z^{(1)}$ would not be appropriate. For an illumination in total internal reflection [Fig. 2(b)], Im(G_{zz}) and Im(G_{xx}) are peaked around $x=0$, Im(G_{zz}) being almost symmetric but in contrast reversal. Moreover, as for normal incidence, Im(G_{yy}) only exhibits suprawavelength variations, with a very low contrast. In summary, Eq. (6) and Fig. 2 demonstrate a very strong polarization effect in near-field phase imaging. They also indicate the circumstances under which the phase variations will follow the *equivalent* surface profile of the object.

In order to check and illustrate the conclusions of the above model, we present exact numerial simulations of the

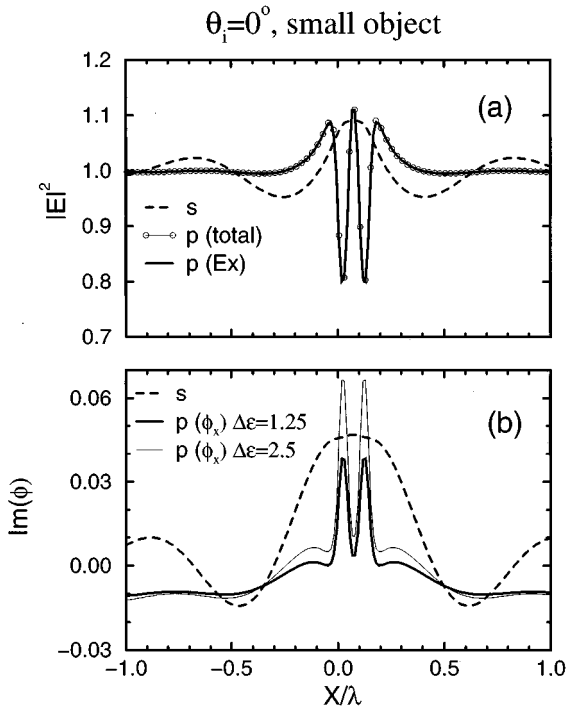

FIG. 3. Numerical calculation of the field along the line $z_0=40$ nm above the sample in Fig. 1. $w=l=h=30$ nm. $\theta_i=0°$. (a) $|E_y|^2$ in s polarization (dashed line), $|\mathbf{E}|^2$ (line with circles) and $|E_x|^2$ (solid line) in p polarization. (b) ϕ_y in s polarization (dashed line), ϕ_x in p polarization with $\Delta\epsilon=1.25$ (bold solid line) and $\Delta\epsilon=2.5$ (thin solid line).

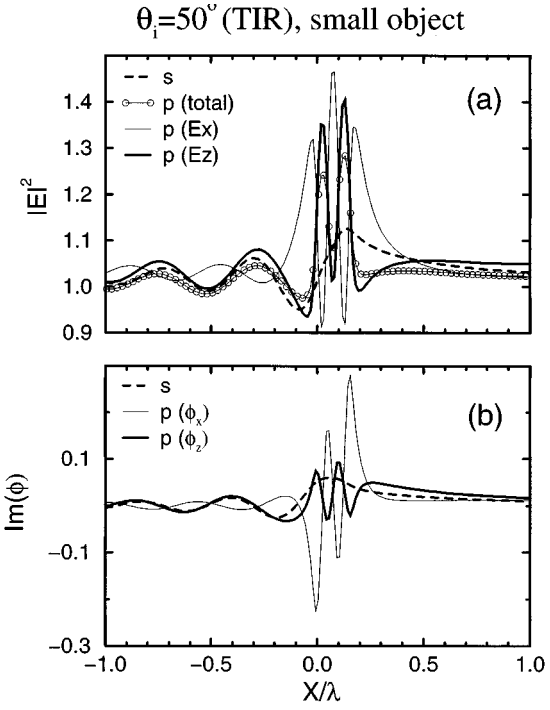

FIG. 4. same as Fig. 3 with $\theta_i=50°$ (total internal reflection). $|E_z|^2$ and $\mathrm{Im}\phi_z^{(1)}$ are also displayed in p polarization.

field scattered by the sample in Fig. 1. The numerical scheme consists of solving Eq. (1) using a moment method, without any approximation. This scheme is described in Ref. [16]. For the sake of computer time and memory space, the geometry is two-dimensional (i.e., invariant along y). All quantities are calculated along a line at a constant height $z=z_0$.

We show in Fig. 3(a) the intensity ($|\mathbf{E}|^2$) calculated for $z_0=40$ nm, in both s (TE) and p (TM) polarizations. The structure is homogeneous ($\epsilon=\epsilon_s=2.25$), with $w=h=l=30$ nm. It is illuminated at normal incidence with a monochromatic plane wave of wavelength $\lambda=633$ nm. The light intensity is more confined around the structure in p (in contrast reversal) than in s polarization, in agreement with calculations previously reported [6]. Moreover, the intensity of the total vector field and that of the x-component alone are practically identical in p polarization. This confirms the hypothesis of weak cross-polarization scattering that was made in our model [see Eq. (2)]. At normal incidence, the incident field is polarized in the x direction, and the total field remains (in a very good approximation) polarized in the same direction.

Figure 3(b) represents the phase $\mathrm{Im}(\phi_y^{(1)})$ in s polarization (dashed curve) and $\mathrm{Im}(\phi_x^{(1)})$ in p polarization (solid bold curve). According to the model presented previously, the phase follows the object structure in p polarization [G_{xx} is implied; see Eq. (6) and Fig. 2(a)], and does not follow the structure in s polarization (G_{yy} is implied). In fact, the phase in s polarization does not exhibit any subwavelength variation. Moreover, in the case of an inhomogeneous sample with dielectric contrast $\Delta\epsilon=\epsilon-1$ increased by a factor of 2 ($\epsilon=3.5$, $\epsilon_s=2.25$), the phase variation also increases by a factor of 2 (solid thin line). This is in agreement with Eq. (6), which shows that the phase variation is proportional to the *equivalent* surface profile.

We show in Fig. 4 the results for an illumination in total internal reflection. The illuminating field $\mathbf{E}^{(0)}$ is in this case an evanescent wave, as in photon scanning tunneling microscopy [7,10]. The results for the intensity are plotted in Fig. 4(a). In s polarization, the situation is unchanged in comparison to the illumination in transmission. In p polarization, the incident field has two nonvanishing components E_x and E_z, and so has the total field. The square modulus of the electric vector field follows more or less the structure, without any contrast reversal. Moreover, the variations of $|E_x|^2$ and $|E_z|^2$ clearly demonstrate that this effect mainly stems from the z component. This was explained theoretically and demonstrated experimentally [5,7]. What is striking is that the same confinement occurs for the phase, as shown in Fig. 4(b). The phase of the z component of the field in p polarization follows the lateral variations of the structure (in contrast reversal, according to Fig. 2) with an excellent resolution. Note that the resemblance between the phase variations and the equivalent surface profile is perturbed by the phase of the illuminating field $E_\alpha^{(0)}$, which is nonzero at nonnormal incidence [see Eq. (4)]. In addition, the phase in s polarization does not exhibit any subwavelength variation.

In conclusion, we have demonstrated that the near-field phase exhibits polarization and confinement effects, similar to those already known for the intensity. An important result is that, for an illumination at normal incidence, the phase of the parallel component of the total field follows the equivalent surface profile with an excellent resolution. For an inci-

dence in total internal reflection, the phase of the normal component of the total field follows the equivalent surface profile in inverse contrast. We have presented a model, based on the Rytov approximation for electromagnetic vector fields, which contains the essential physics of the phase behavior in the near-field zone. It describes the polarization effects. It also explains how the topographic and dielectric constant variations of the object influence the phase of the near field. This is a very important point in SNOM, where the purely optical properties of the sample are of great interest. The conclusions of our model have been illustrated by exact numerical simulations of the near field scattered by two-dimensional structures of nanometric dimensions.

Finally, we would like to show that the observed polarization and confinement effects are pure near-field effects that are encountered in the scattering by nanometric structures only. Figure 5 shows the phase $\mathrm{Im}\phi_y^{(1)}$ and $\mathrm{Im}\phi_x^{(1)}$ in *s* and *p* polarization, respectively [as in Fig. 3(b)], for the sample in Fig. 1 with $h=63$ nm, $w=633$ nm, and $l=2.5$ μm. It can be seen that the phase in *s* and *p* polarizations are very similar, both of them following the sample structure. This is precisely the result that is predicted by a scalar description of the field, as in physical optics [17]. Thus, with increasing the structure lateral size up to one wavelength or more, i.e., by reaching the domain of physical optics, the polarization-dependent phase confinement effect disappears.

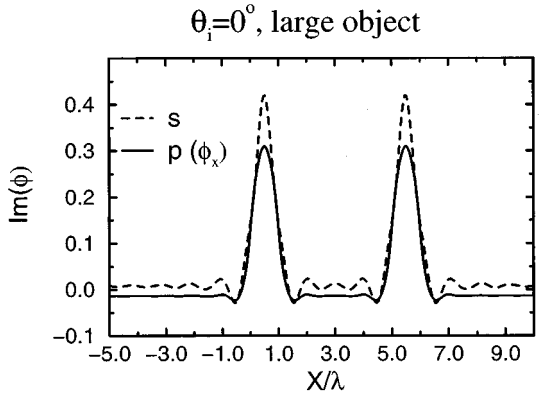

FIG. 5. ϕ_y in *s* polarization and ϕ_x in *p* polarization for the sample in Fig. 1 with $w=633$ nm, $h=63$ nm, $l=2.5$ μm, and $z_0=175$ nm. $\theta_i=0°$.

I would like to thank the EC for financial support. Helpful discussions with N. García, J.-J. Greffet, A. Sentenac, and M. Nieto-Vesperinas are also appreciated.

[1] E. A. Ash and G. Nicholls, Nature (London) **237**, 510 (1972).

[2] D. W. Pohl, W. Denk, and M. Lanz, Appl. Phys. Lett. **44**, 651 (1984); E. Betzig, M. Isaacson, and A. Lewis, *ibid.* **51**, 2088 (1987).

[3] C. Girard and A. Dereux, Rep. Prog. Phys. **59**, 657 (1996).

[4] D. Van Labeke and D. Barchiesi, J. Opt. Soc. Am. A **9**, 732 (1992); **10**, 2193 (1993).

[5] O. J. F. Martin, C. Girard, and A. Dereux, Phys. Rev. Lett. **74**, 526 (1995); C. Girard, A. Dereux, O. J. F. Martin, and M. Devel, Phys. Rev. B **52**, 2889 (1995).

[6] J.-J. Greffet and R. Carminati, in *Optics at the Nanometer Scale*, edited by M. Nieto-Vesperinas and N. García (Kluwer, Dordrecht, 1996), p. 1.

[7] J. C. Weeber, E. Bourillot, A. Dereux, J. P. Goudonnet, Y. Chen, and C. Girard, Phys. Rev. Lett. **77**, 5332 (1996).

[8] M. Totzeck and M. A. Krumbügel, Opt. Commun. **112**, 189 (1994); F. Keilman *et al.*, *ibid.* **129**, 15 (1996).

[9] F. Zenhausern,Y. Martin, and H. K. Wickramasinghe, Science **269**, 1083 (1995).

[10] C. Bainier, D. Courjon, F. Baida, and C. Girard, J. Opt. Soc. Am. A **13**, 267 (1996).

[11] N. García and M. Nieto-Vesperinas, Appl. Phys. Lett. **66**, 3399 (1995).

[12] The Rytov approximation for scalar fields was used in Ref. [11].

[13] A. Poggio and E. Miller, in *Computer Techniques for Electromagnetics*, edited by R. Mittra (Pergamon Press, Oxford, 1973).

[14] M. Nieto-Vesperinas, *Scattering and Diffraction in Physical Optics* (Wiley, New York, 1991), Chap. 3, p. 112.

[15] R. Carminati and J.-J. Greffet, J. Opt. Soc. Am. A **11**, 2716 (1995); Ultramicroscopy **61**, 43 (1995).

[16] F. Pincemin, A. Sentenac, and J.-J. Greffet, J. Opt. Soc. Am. A **11**, 1117 (1994); F. Pincemin, A. A. Maradudin, A. D. Boardman, and J.-J. Greffet, Phys. Rev. B **50**, 15261 (1994).

[17] J. W. Goodman, *Introduction to Fourier Optics* (McGraw-Hill, New York, 1968), Chap. 5, p. 77.